Continuum theory of axial segregation in a long rotating drum

I. S. Aranson,[1] L. S. Tsimring,[2] and V. M. Vinokur[1]
[1]*Argonne National Laboratory, 9700 South Cass Avenue, Argonne, Illinois 60439*
[2]*Institute for Nonlinear Science, University of California, San Diego, La Jolla, California 92093-0402*
(Received 29 March 1999)

We develop a continuum description for the axial segregation of granular materials in a long rotating drum based on the dynamics of the thin near-surface granular flow coupled to bulk flow. The equations of motion are reduced to the one-dimensional system for two local variables only, the concentration difference and the dynamic angle of repose, or the average slope of the free surface. The parameters of the system are established from comparison with experimental data. The resulting system describes both initial transient traveling wave dynamics and the formation of quasi-stationary bands of segregated materials. A long-term evolution proceeds through slow logarithmic coarsening of the band structure which is analogous to the spinoidal decomposition described by the Cahn-Hilliard equation. [S1063-651X(99)08508-6]

PACS number(s): 45.70.−n, 47.54.+r

I. INTRODUCTION

The collective dynamics of granular materials is a subject of current interest [1–6]. The intrinsic dissipative nature of the interactions between the constituent macroscopic particles gives rise to several basic properties specific to granular substances and setting granular matter apart from the conventional gaseous, liquid, or solid states. One of the most fascinating features of heterogeneous (i.e., consisting of different distinct components) granular materials is their ability to segregate under the external agitation rather than to further mix, as one would expect from the naive entropy consideration. In fact, any variation in mechanical properties of particles (like size, shape, density, surface roughness) may lead to their segregation. Segregation has been observed in most flows of granular binary mixtures, including granular convection [7], hopper flow [8,9], and flows in rotating drums [3,4,6]. Mixtures of grains with different sizes in long rotating drums exhibit both radial and axial size segregation [3,4,6,10]. In case of radial segregation the grains of one type (for grains of different sizes, the smaller ones) rapidly build up a core near the axis of rotation. This radial separation is often followed by slow axial segregation, with the mixture of grains separating into the pure bands arranged along the axis of the drum. Axial segregation leads to either a stable array of concentration bands, or, after a very long time, to complete segregation [11].

The granular dynamics in a slowly rotating drum, although resembling viscous fluid flow, has its very special distinctive features. In the bulk, the granular material rotates almost as a solid with some internal slipping. As moving grains reach the free surface they slide down within a thin near-surface layer [5]. At an intermediate rotation speed, the surface has a nearly flat *S*-curved shape; the arctangent of its average slope defines the so-called *dynamic angle of repose*. Since there is almost no shear flow in the bulk, the segregation predominantly occurs within this thin fluidized near-surface layer, the particles being advected into the bulk by the radial rotation. The radial segregation occurs during the first few revolutions of the drum. For long narrow drums with the length much exceeding the radius, radial segregation is accompanied by *axial segregation* occurring at later stages (after several hundreds of revolutions). Recent experiments [3,4,6,10] have revealed the interesting new features of axial segregation: At early stages, the small-scale perturbations propagate across the drum in both directions (this was clearly evidenced by the experiments on the dynamics of presegregated mixtures [6]), while at later times more long-scale static perturbations take over and lead to emergence of quasistationary bands of separated grains. Bands of segregated materials interact at a very long time scale and exhibit very slow coarsening [4,10,11]. Depending on the experimental conditions, such as the speed of rotation, type of grains, etc., the final state can be either a small number of stationary bands [10] or two completely segregated bands [11]. This latter process can be accelerated in a drum of a helicoidal shape [4]. Bands can also be locked in a drum with the radius modulated along the axis [4].

Most of the theoretical models agree on the fact that the underlying reason for segregation is the sensitive dependence of the surface slope and/or shape upon the relative concentration of different particles in the mixture [4,12–16]. In Ref. [4] a simple theory of segregation due to surface flow driven by the local profile was proposed. The dynamics of a binary mixture is described by a nonlinear diffusion equation for the relative concentration of the ingredients along the horizontal axis. Axial segregation occurs then when the diffusion coefficient turns negative. This model yields a significant insight into the nature of the instability leading to the segregation, but being based on a first-order diffusion equation, it fails to describe the traveling waves observed at the early stages of axial segregation [6,10].

In this paper we develop a continuum description of the axial size segregation in long rotating drums based on the simplified transport equations following from the conservation laws for the binary mixture of granular particles. We show that under certain assumptions these equations are reduced to a system of only two coupled one-dimensional partial differential equations for two dynamic variables: the dynamic angle of repose and the concentration difference averaged over the cross section of the drum. This simplified model describes consistently the early phase of segregation

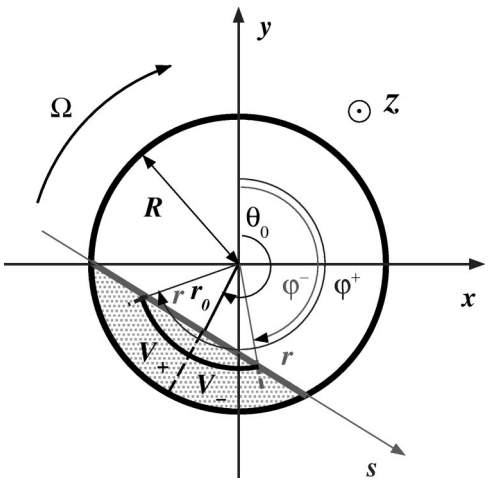

FIG. 1. Sketch of the rotating drum cross section (z coordinate along the drum axis is directed perpendicular to the figure plane). Here Ω is the angular velocity, R is the external radius of drum, r_0, θ_0 are polar coordinates of the point on the free surface at the minimum distance from the axis of drum, s is the coordinate along free surface of the drum, and $\phi^{\pm}$ are the polar angles of the points on the free surface at a distance r from the axis. $V_{\pm}$ indicate the upper/lower halves of the filled part of drum.

with traveling waves as well as the later stage of segregation characterized by slow merging of bands of different particles. Our model predicts slow (logarithmic) coarsening of the segregated state. The dynamics of segregation shows striking similarity with the experiments of Ref. [6]. The preliminary account of some of our results derived within the phenomenological model was presented in Ref. [12].

The structure of the paper is the following. In Sec. II we formulate the problem and discuss assumptions used in our theory. In Sec. III we introduce transport equations in which the three-dimensional flow of granular material in the drum is divided into a bulk flow and near-surface boundary layer. In Sec. IV we reduce the three-dimensional model to a one-dimensional system for only two dynamic variables: the local angle of repose and the relative concentration difference. In Sec. V we consider the stability of a uniform mixed state and derive a dispersion relation for small perturbations. In Sec. VI we compare the theoretical results with the experimental data of Ref. [6]. In Sec. VII we present the numerical analysis of time evolution of the axial segregation described by the one-dimensional model. In Sec. VIII we consider long-time behavior of band coarsening and present analytical estimates for the number of bands as function of time. Conclusion discusses the possible generalizations of our results. In the Appendix we present the derivation of the asymptotic structure of a single front between two bands of different grains.

II. FORMULATION OF THE PROBLEM AND SIMPLIFYING ASSUMPTIONS

The geometry of the problem is shown in Fig. 1. We consider a mixture of two kinds of particles, 1 and 2, of which 1(2) corresponds to particles with larger (smaller) static repose angle θ_1 (θ_2), placed in a horizontal rotating cylinder. The volume concentrations of particles are $c_{1,2}$. In addition to a standard Cartesian coordinate frame (x,y,z) we introduce a local orthogonal coordinate frame on the free surface (s,z), where the origin O, $s=0$, corresponds to the middle line or locus of points on the surface closest to the rotation axis and the s-axis itself is perpendicular to the drum radius pointing to the middle point $r=r_0$ (see Fig. 1). The shape of the free surface is defined via two functions $\phi^+(r,z,t)$ and $\phi^-(r,z,t)$ for the top and bottom parts of the surface with respect to the middle point $r=r_0$. We build our model on the following assumptions.

(i) The mass of grains in each cross-section of the drum remain constant. This conservation law is maintained by the bulk flow which in the rapidly rotating drums deviates substantially from a simple solid rotation (cf. Ref. [4]).

(ii) Particle volume concentrations $c_{1,2}$ do not depend on transverse coordinates r, ϕ and are only functions of axial coordinate z. This assumption is justified for rapidly rotating drums of small radii (such as those used in Ref. [6]), where the strong bulk flow and Fick diffusion may prevent the radial segregation while the axial segregation still occurs because it develops on a much larger length scale.

(iii) The grains segregate predominantly near the surface of the drum, whereas in the bulk of the drum particles are equally advected by the bulk flow. This assumption stems from the fact that phase separation requires the dilation of the granular matter, and this dilation takes place mainly within the near-surface boundary layer.

(iv) The shape of the free surface in each cross-section of the drum are approximated by a straight line. We show that indeed the axial segregation can occur even for a straight profile of free surface provided that the filling ratio of the grains is different from 50%.

(v) Densities of both sorts of particles are equal and, therefore, can be excluded from the theory.

III. TRANSPORT EQUATIONS

Let us consider the mechanisms of mass transport contributing to the normal displacement of the free surface of the rotating drum. We divide the interior of the drum in two parts—the bulk and the near-surface boundary layer. In the boundary layer, the granular material is strongly dilated. The dilation of the surface layer leads to the separation of the binary granular material. In the bulk of the drum, the granular material is densely packed, and both sorts of particles are advected by the granular flow without significant segregation. The mass transport in the rotating drum is controlled by the fluxes of the particles both in the bulk and in the near-surface flow. Let us consider two tubes of a unit cross-section along polar arc ϕ at a radius $r>r_0$, extending from $\phi=\theta_0$ to $\phi^{\pm}$, where $\phi^{\pm}$ correspond to the surface, and constant θ_0 indicates an angle which initially divides the cross-section of the drum in the halves of equal area $V_{\pm}$ (see Fig. 1). The total mass of the granular material of ξ in the tubes is

$$\xi^+ = r(\phi^+ - \theta_0), \qquad \xi^- = -r(\phi^- - \theta_0) \tag{1}$$

(we assume unit volume density of the granular media). The partial masses of each sort of particles $\xi^{\pm}_{1,2}$ are defined as

follows $\xi^{\pm}_{1,2}=c_{1,2}\xi^{\pm}$. The equations for $\xi^{\pm}_{1,2}$ following from the mass conservation law, can be written in the form:

$$\partial_t \xi_i^+ = -\int_{\theta_0}^{\phi^+} d\phi \mathrm{div}\mathbf{b}_i - \frac{1}{\sin\psi^+}\mathrm{div}^s \mathbf{j}_i^+ , \tag{2}$$

$$\partial_t \xi_i^- = -\int_{\phi^-}^{\theta_0} d\phi \mathrm{div}\mathbf{b}_i - \frac{1}{\sin\psi^-}\mathrm{div}^s \mathbf{j}_i^- , \quad i=1,2. \tag{3}$$

Here $\mathbf{b}_i$ is the bulk flux of the ith granular component, and $\mathbf{j}_i^{\pm}$ are the surface fluxes integrated across the boundary layer at points $\phi^{\pm}$. We assume that the bulk fluxes of particles $\mathbf{b}_{1,2}$ of each type are determined by the condition

$$\mathbf{b}_{1,2}=c_{1,2}\mathbf{b}, \tag{4}$$

where $\mathbf{b}$ is the total flux of both components in the bulk. Condition (4) implies that particles are simply advected by the bulk flow without segregation. Although the bulk flux may have a rather complicated three-dimensional structure, as we will show later on, the condition of the z-independence of the number of the particles in each cross section of the drum allows to express the bulk flux in terms of integral of surface flux. Thus, detailed structure of the bulk flux is not important in the framework of our approximations.

Surface fluxes $\mathbf{j}_{1,2}$ are comprised of the convective part which depends on the local slope of the surface ∇y and local relative concentrations $c_{1,2}$, and the diffusive part which is caused be multiple particle collisions,

$$\mathbf{j}_{1,2}=-c_{1,2}\alpha\frac{\nabla y}{|\nabla y|}(|\nabla y|-\tan\theta_{1,2})-K_{1,2}\nabla c_{1,2}, \tag{5}$$

where $\theta_{1,2}$ are the static repose angles of the two components, and $K_{1,2}$ are (generally, different) Fick's diffusion constants. For the convective part of the flux Eq. (5) we adopted the linearized expression from Ref. [4], where the proportionality constant α was found in the form $\alpha=gd_0^3/3\eta$. Here g is gravity acceleration, η is friction coefficient, d_0 is the ''effective'' layer thickness. The vector of the local slope is determined by

$$\nabla y=\frac{\partial_s y}{\sqrt{1-\partial_s y^2}}\hat{\mathbf{s}}+\partial_z y\hat{\mathbf{z}}, \tag{6}$$

where $\hat{\mathbf{z}}$ and $\hat{\mathbf{s}}$ are locally orthogonal unit vectors along the axis of the cylinder and the free surface. The two-dimensional (2D) divergence operator $\mathrm{div}^s=\hat{\mathbf{s}}\partial_s+\hat{\mathbf{z}}\partial_z$ applies only on the free surface of the drum. In Eqs. (2) and (3), $\psi^{\pm}$ are the angles between the unit vector $\hat{\boldsymbol{\phi}}$ and the normal to the surface at $\phi=\phi^{\pm}$, and it is easy to see that

$$\sin\psi^{\pm}=\frac{1}{\sqrt{1+(r\partial_r\phi^{\pm})^2}}. \tag{7}$$

In the following we will assume the free surface to be flat,

$$y=r_0\sqrt{1+k^2}-kx, \tag{8}$$

where r_0 is the distance between the middle point $s=0$ and the drum axis and $k=\tan\theta_0$ is the slope. In this case both angles $\psi^{\pm}$ are equal, and

$$\sin\psi^{\pm}=\sqrt{1-r_0^2/r^2}. \tag{9}$$

The 2D divergence operator div^s can be rewritten in polar coordinates as

$$\mathrm{div}^s\mathbf{j}^{\pm}=\mp\sqrt{1-r_0^2/r^2}\partial_r j_s^{\pm}+\partial_z j_z^{\pm}, \tag{10}$$

where $j_s^{\pm}, j_z^{\pm}$ are components of the total surface flux along s and z directions, respectively.

The equation for the total mass of granular material of sort i in the tube from ϕ^- to ϕ^+, $\mu_i=c_i r(\phi^+-\phi^-)$, $i=1,2$, is obtained by summing Eqs. (2) and (3), and making use of Eqs. (1) and (9),

$$\partial_t\mu_i=-\frac{1}{\sqrt{1-r_0^2/r^2}}\mathrm{div}^s(\mathbf{j}_i^+ + \mathbf{j}_i^-)-\int_{\phi^-}^{\phi^+} d\phi \mathrm{div}\mathbf{b}_i . \tag{11}$$

In order to derive the equation for the local dynamic repose angle we subtract (3) from (2), and add the resulting equations for c_1 and c_2,

$$r\partial_t(\phi^+ + \phi^-)=-\frac{1}{\sqrt{1-r_0^2/r^2}}\mathrm{div}^s(\mathbf{j}^+ - \mathbf{j}^-)-\int_{\theta_0}^{\phi^+} d\phi \mathrm{div}\mathbf{b} + \int_{\phi^-}^{\theta_0} d\phi \mathrm{div}\mathbf{b}. \tag{12}$$

Here we used the incompressibility condition for the bulk concentrations (compare [4,13]):

$$c_1+c_2=1. \tag{13}$$

and used notation $\mathbf{j}^{\pm}=\mathbf{j}_1^{\pm}+\mathbf{j}_2^{\pm}$ for the surface fluxes of both components.

The integrals over divergences of the bulk flow can be evaluated only if the structure of the bulk flow is known. For a slow drum rotation, the bulk is involved in a divergence-free rigid body rotation $[\mathbf{b}=(b_\phi,b_r)=(\Omega r,0)]$ and a small axial backflow which compensates mass transport by the surface flux. In this case the integrals are reduced to the fluxes through the cross section of the tube at $\phi=\theta_0$ (since at free surface $\mathbf{b}=0$),

$$\int_{\theta_0}^{\phi^{\pm}} d\phi \mathrm{div}\mathbf{b}_{1,2}=-c_{1,2}\Omega+\partial_z c_{1,2}B_z . \tag{14}$$

Here $B_z^{\pm}=\int_{\theta_0}^{\phi^{\pm}} d\phi b_z$. For a fast drum rotation, the bulk flow deviates from purely azimuthal motion and it reduces significantly the portion of the grains brought by the bulk flow to the surface boundary layer. In the absence of detailed knowledge about the structure of the bulk flow, we describe this reduction by a constant parameter ϵ:

$$\int_{\theta_0}^{\phi^{\pm}} d\phi \mathrm{div}\mathbf{b}_{1,2} \approx -\epsilon c_{1,2}\Omega + \partial_z c_{1,2} B_z, \tag{15}$$

where for slow rotation $\epsilon \to 1$, and for fast rotation, $\epsilon \ll 1$.

IV. ONE-DIMENSIONAL MODEL

A. Relative concentration

We define an average over a cross section as

$$\langle A \rangle = \frac{2}{R^2 - r_0^2} \int_{r_0}^{R} A r dr. \tag{16}$$

After integration of the bulk flux over the cross section, we obtain the following equations:

$$\Phi \partial_t c_1 = -\left\langle \frac{1}{\sqrt{r^2 - r_0^2}} \partial_z j_{1z} \right\rangle - \partial_z \langle c_1 B_z \rangle, \tag{17}$$

$$\Phi \partial_t c_2 = -\left\langle \frac{1}{\sqrt{r^2 - r_0^2}} \partial_z j_{2z} \right\rangle - \partial_z \langle c_2 B_z \rangle, \tag{18}$$

where $B_z = B_z^+ + B_z^-$ is the total z component of the averaged bulk flow $\mathbf{B}$, $j_{iz} = j_{iz}^+ + j_{iz}^-$, and $\Phi = \langle \phi^+ - \phi^- \rangle$ is related to the filling ratio ζ as $\Phi = \zeta 2\pi R^2/(R^2 - r_0^2)$. For a flat profile and $r_0 \ll R$, $\Phi \approx \pi - 4r_0/R$. Thus, assuming $r_0 \ll 1$ we obtain $\zeta = 1/2 - 2r_0/\pi R$. The condition that the total number of particles in each cross section is a constant, leads to the relation $\langle B_z \rangle = -\langle (j_{1z} + j_{2z})/\sqrt{r^2 - r_0^2} \rangle$ (cf. [4]). Subtracting (18) from (17), we arrive at the equation for the relative concentration $C = c_1 - c_2$,

$$\Phi \partial_t C = -\left\langle \frac{1}{\sqrt{r^2 - r_0^2}} \partial_z [(1-C) j_{1z} - (1+C) j_{2z}] \right\rangle. \tag{19}$$

The mass conservation in each cross section for flat surface implies $r_0 = \text{const}$. We can express $x^{\pm}, y^{\pm}$, and $\phi^{\pm}$ in terms of θ and r,

$$\phi^{\pm} = \pi/2 + \theta \pm \arccos r_0/r, \tag{20}$$

$$x^{\pm} = r \sin \phi^{\pm} = -r_0 \sin\theta \mp \cos\theta \sqrt{r^2 - r_0^2}, \tag{21}$$

$$y^{\pm} = r \cos \phi^{\pm} = -r_0 \cos\theta \pm \sin\theta \sqrt{r^2 - r_0^2}. \tag{22}$$

The expression for the fluxes (5) can be further simplified assuming that slope along z y_z is much smaller than slope along x, which is $\tan\theta$, yielding

$$j_{1,2z} \approx -\alpha c_{1,2} \partial_z y \left[1 - \frac{\tan\theta_{1,2}}{\tan\theta} \right] - K_{1,2} \partial_z c_{1,2}, \tag{23}$$

$$j_{1,2r} \approx -\frac{\alpha c_{1,2}}{\sqrt{r^2 - r_0^2}} (\tan\theta - \tan\theta_{1,2}). \tag{24}$$

Using these expressions, we can rewrite Eq. (19) as

$$\partial_t C = -\frac{\alpha}{2\Phi} (\tan\theta_2 - \tan\theta_1) \partial_z \left[(1-C^2) \left\langle \frac{1}{\sqrt{r^2 - r_0^2}} \frac{\partial_z (y^+ + y^-)}{\tan\theta} \right\rangle \right] + \frac{2\partial_z [(K_1(1+C) + K_2(1-C)) \partial_z C]}{\Phi \sqrt{R^2 - r_0^2}}. \tag{25}$$

For $r_0 = 0$ the first term on the right-hand side (rhs) of Eq.(25) turns into zero, and one has to take into account higher order corrections to the flat profile (see [4]). However, for $r_0 \neq 0$ (not 50% filling ratio), the axial component of the convective component of the surface flux is nonzero even if the profile is flat, since

$$\left\langle \frac{1}{\sqrt{r^2 - r_0^2}} \frac{y_z^+ + y_z^-}{\tan\theta} \right\rangle = -\frac{4r_0}{\sqrt{R^2 - r_0^2} \tan\theta} \partial_z \cos\theta. \tag{26}$$

Taking into account (26) and introducing notation $\beta = (\tan\theta_1 - \tan\theta_2)/2$, we derive finally

$$\partial_t C = -\frac{4\alpha\beta r_0}{\Phi \sqrt{R^2 - r_0^2}} \partial_z \left[\frac{(1-C^2)}{\tan\theta} \partial_z \cos\theta \right] + \frac{2\partial_z [(K_1(1+C) + K_2(1-C)) \partial_z C]}{\Phi \sqrt{R^2 - r_0^2}}. \tag{27}$$

B. Dynamic repose angle

Let us introduce the local dynamic repose angle as

$$\theta = \frac{1}{2} \langle \phi^+ + \phi^- \rangle - \pi. \tag{28}$$

For flat surface (8), $\theta = \arctan k$. The equation for the dynamic repose angle can be obtained by averaging Eq. (12),

$$\partial_t \theta = \epsilon\Omega - \tfrac{1}{2} \partial_z \langle B_z^+ - B_z^- \rangle - \frac{2\alpha}{R^2 - r_0^2} (\tan\theta - \tan\theta_0 - \beta C) - \left\langle \frac{1}{2\sqrt{r^2 - r_0^2}} \partial_z (j_z^+ - j_z^-) \right\rangle. \tag{29}$$

Here $\tan\theta_0 = (\tan\theta_1 + \tan\theta_2)/2$. The first two terms on the r.h.s. of Eq.(29) are obtained by integration over the divergence of the bulk flux (15). The third term stems from the radial component of the surface flux, and the last term is

obtained from the axial component of the surface flux. To derive Eq. (29) we have used the natural boundary conditions $j_s^+(r_0)=j_s^-(r_0), j_s^+(R)=j_s^-(R)=0$. For lack of a better knowledge of the structure of the bulk flow, we assume that the difference of the axial bulk flows in the upper and lower parts $\langle B_z^+ - B_z^- \rangle$ is proportional to the total bulk flow $\langle B_z \rangle$. Then the corresponding term in this equation can be expressed as

$$\langle B_z^+ - B_z^- \rangle = \kappa \langle B_z \rangle = -\frac{4\kappa\alpha r_0}{\sqrt{R^2-r_0^2}}\left(1-\frac{\tan\theta_0+\beta C}{\tan\theta}\right)\partial_z(\cos\theta)+\frac{2\kappa(K_1-K_2)}{\sqrt{R^2-r_0^2}}\partial_{zz}^2 C, \tag{30}$$

where κ is the proportionality constant. In principle, κ can be evaluated if the detailed structure of bulk flow is known. Later on we will estimate κ from the fitting to experimental data.

Using Eqs.(22),(23) we obtain from (29)

$$\partial_t\theta=\epsilon\Omega-\frac{2\alpha}{R^2-r_0^2}(\tan\theta-\tan\theta_0-\beta C)+\alpha\partial_z\left[\left(1-\frac{\tan\theta_0+\beta C}{\tan\theta}\right)\left(\cos\theta-\frac{2\kappa r_0\sin\theta}{\sqrt{R^2-r_0^2}}\right)\partial_z\theta\right]+\frac{\kappa(K_1-K_2)}{\sqrt{R^2-r_0^2}}\partial_z^2 C. \tag{31}$$

This equation together with the equation for the relative concentration C

$$\partial_t C=-\frac{4\alpha\beta r_0}{\Phi\sqrt{R^2-r_0^2}}\partial_z[(1-C^2)\cos\theta\partial_z\theta]+\frac{2\partial_z[(K_1+K_2-(K_1-K_2)C)\partial_z C]}{\Phi\sqrt{R^2-r_0^2}} \tag{32}$$

comprise a complete set of equations for the grain separation in the rotating drum.

C. Simplified equations

Equations (31) and (32) can be substantially simplified if one takes into account that the angle θ changes within a very small range. Then one can linearize the equations with respect to θ near θ^*, where θ^* is the dynamic repose angle corresponding to uniformly mixed state. However, we will retain nonlinearity in C, since C changes from -1 to 1. The value of θ^* for $C=0$ is obtained from

$$\tan\theta^*=\frac{\epsilon\Omega(R^2-r_0^2)}{2\alpha}+\tan\theta_0. \tag{33}$$

We introduce a new variable $\Theta=\theta-\theta^*$ and keep only terms linear in Θ. Then Eqs. (31) and (32) can be written as

$$\partial_t\Theta=-\overline{\alpha}(\Theta-\overline{\beta}C)+D_\theta\partial_z^2\Theta+D\partial_z^2 C,$$

$$\partial_t C=-\delta\partial_z[(1-C^2)\partial_z\Theta]+D_c\partial_z[(1-\eta C)\partial_z C]. \tag{34}$$

where the coefficients are expressed as follows:

$$\overline{\alpha}=\frac{2\alpha}{R^2-r_0^2}\cos^{-2}\theta^*,$$

$$\overline{\beta}=\frac{\tan\theta_1-\tan\theta_2}{2}\cos^2\theta^*,$$

$$D_\theta=\frac{1}{2}\epsilon\Omega(R^2-r_0^2)\frac{\cos\theta^*}{\sin\theta^*}\left(\cos\theta^*-\frac{2\kappa r_0\sin\theta^*}{\sqrt{R^2-r_0^2}}\right),$$

$$D=\frac{\kappa(K_1-K_2)}{\sqrt{R^2-r_0^2}},$$

$$D_c=2\frac{K_1+K_2}{\Phi\sqrt{R^2-r_0^2}},$$

$$\delta=\frac{2\alpha r_0\cos\theta^*(\tan\theta_1-\tan\theta_2)}{\Phi\sqrt{R^2-r_0^2}},$$

$$\eta=\frac{K_1-K_2}{K_1+K_2}. \tag{35}$$

In the derivation of Eqs. (34) we neglected nonlinear terms $\sim\beta C\partial_z\theta$ since $\overline{\beta}\ll\tan\theta_0$. This system was first introduced phenomenologically in our preliminary publication [12].

V. LINEAR STABILITY OF A MIXED STATE

Equations (34) possess a steady solution, corresponding to a uniform mixed state:

$$\Theta=0, \quad C=C_0. \tag{36}$$

After linearization we obtain the following equations for small perturbations with respect to this solution:

$$\partial_t\Theta=-\overline{\alpha}(\Theta-\overline{\beta}C)+D\partial_z^2 C+D_\theta\partial_z^2\Theta, \tag{37}$$

$$\partial_t C=-\overline{\delta}\partial_z^2\Theta+\overline{D}_c\partial_z^2 C, \tag{38}$$

where

$$\overline{D}_c=D_c(1-\eta C_0),$$

$$\overline{\delta}=\delta(1-C_0^2) \tag{39}$$

[we kept the same notations θ and C for the perturbations to the uniform state (36)]. Representing the solution to Eqs. (37) and (38) in the form $\theta, C \sim \exp[ikz+\lambda t]$ we obtain an expression for the growth rate λ:

$$\lambda = -\frac{\overline{\alpha}+(D_\theta+\overline{D}_c)k^2}{2} \pm \sqrt{\frac{(\overline{\alpha}+(D_\theta-\overline{D}_c)k^2)^2}{4}+\overline{\alpha\beta\delta}k^2-D\overline{\delta}k^4}. \quad (40)$$

In the limit $k\to 0$ one of the roots of Eq. (40) is large and negative, whereas the other root is given by

$$\lambda = (\overline{\beta\delta}-\overline{D}_c)k^2+O(k^4). \quad (41)$$

Segregation occurs only if $\beta\overline{\delta}>\overline{D}_c$. Using expressions from Eqs. (35) we obtain the explicit condition for the onset of segregation in terms of repose angles (for simplicity we take $C_0=0$):

$$(\tan\theta_1-\tan\theta_2)^2>2\frac{K_1+K_2}{\alpha r_0\cos^3\theta^*}. \quad (42)$$

As we can see from Eq. (42) axial segregation occurs only if the difference of partial repose angles $\theta_{1,2}$ exceeds some critical value determined by Fick diffusion coefficients.

Let us emphasize some similarity with the results of Ref. [4]. The expression (41) is in fact similar to that of Ref. [4] if we set $D_c=0$ [see Eq. (7) in that paper]. Indeed, if we neglect the time derivative in our Eq. (37), Eq. (38) for the concentration difference in the first order in k^2 can be rewritten as $\partial_t C \approx \delta\partial_z^2\Theta \approx \delta\partial_c\Theta\,\partial_z^2 C$. Now, expressing $\partial_c\Theta$ from Eq. (37), we obtain our result, Eq. (41).

For $k\gg 1$ we obtain

$$\lambda = -\frac{1}{2}(D_\theta+\overline{D}_c)k^2 \pm ik^2\sqrt{\overline{\delta}D-(\overline{D}_c-D_\theta)^2/4}. \quad (43)$$

Therefore, decaying oscillations are possible for large enough k if $\overline{\delta}D>(\overline{D}_c-D_\theta)^2/4$. This is a feature that does not appear in the theory of Zik *et al.* [4]. Equation (43) shows some nontrivial dependence of the threshold for oscillation on concentration C. Making use of Eq. (39) we obtain the condition for oscillations

$$D\delta>\frac{1}{4}\frac{(D_c(1-\eta C_0)-D_\theta)^2}{1-C_0^2}. \quad (44)$$

Since coefficients β, δ, D_c, and D_θ are not dependent on C_0, Eq. (44) gives a condition for onset of transient waves as a function of averaged concentration C. Indeed, if for $C=0$ we have $D\delta<(D_c-D_\theta)/4$, the condition (44) can still be satisfied for $C_0>0$, as was found in experiments [6]. Moreover, our expression (44) predicts that the oscillatory behavior is impossible if $C_0\to\pm 1$.

The full dispersion curve $\lambda(k^2)$ for particular values of the parameters is plotted in Fig. 2. For small wave numbers $0<k<k_c$ there is an instability leading to the stationary separation. The growth rate of the instability reaches maximum at a certain wave number k_m. At larger wave numbers $k>k_*$ (where $k_*>k_c$), perturbations decay and oscillate leading to the occurrence of traveling waves. This picture is consistent with observations of Ref. [6]. In the next section we use the experimental data of Ref. [6] to estimate the parameters of the model, and compare the theory with measurements on a quantitative level.

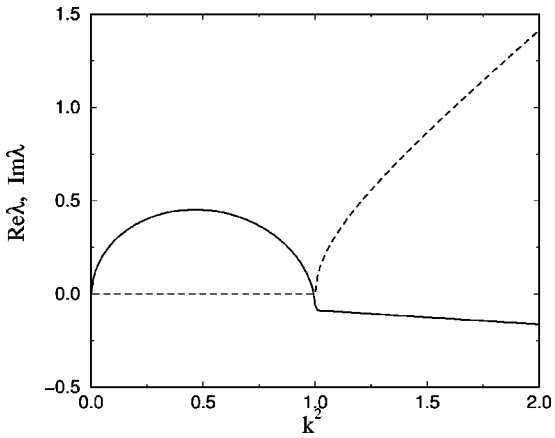

FIG. 2. Dispersion relation $\lambda(k)$ for the small perturbation of the uniform state $C_0=0$ at $\beta=40$, $D_c=0.05$, $D_\theta=0.1$, $\overline{\alpha}=0.025$, $D=1, \overline{\delta}=1, \eta=0$. The solid line represents Reλ, the dashed line represents Imλ. Perturbations are unstable at $k<k_c=0.994$ and oscillate (and decay) at $k>k_*=1$.

VI. COMPARISON WITH THE EXPERIMENTAL DATA

On a qualitative level our model, Eqs. (38), faithfully reproduces the observed phenomenology: transient standing waves, formation of bands, and slow band merging. However, direct quantitative comparison with experiments is difficult since the explicit measurements of some model parameters such as repose angles $\theta_{1,2}$, diffusion coefficients $K_{1,2}$, and α in the range of rotation frequencies Ω are not available yet. Parameters Ω, α are known from experimental conditions (see [6]). Then, the parameters D_θ and δ can be calculated using Eq. (35). The remaining parameters ϵ and D, D_c could be obtain from fitting the dispersion relation for traveling waves measured in Ref. [6]. Unfortunately, from this limited data we cannot obtain reliable estimates for all the parameters. In this section we will present only the order of magnitude values.

In the experiments Ref. [6] the conditions were:

(i) External radius $R=13.5$ mm.

(ii) Filling fraction 0.28 leading to $r_0=4.67$ mm and $\Phi \approx \pi-4r_0/R=1.75$.

(iii) Typical angular frequency $\Omega=4.81$ rad/sec.

(iv) Particles with the typical grain sizes 180 μm (sand) and 425 μm (salt).

Partial repose angles are not known precisely. As an estimate for static repose angles we can take the values from Refs. [4,17], $\theta_1=40°/45°$ and $\theta_2=30°$, leading to the value of parameter $\beta=(\tan\theta_1-\tan\theta_2)/2\approx 0.2$. However, according to [6] for such a high speed of rotation part of the particles goes airborne, suggesting even higher repose angle θ^*. Moreover, effective ''static repose angles'' may not be representative for such high rotation speeds. Although the struc-

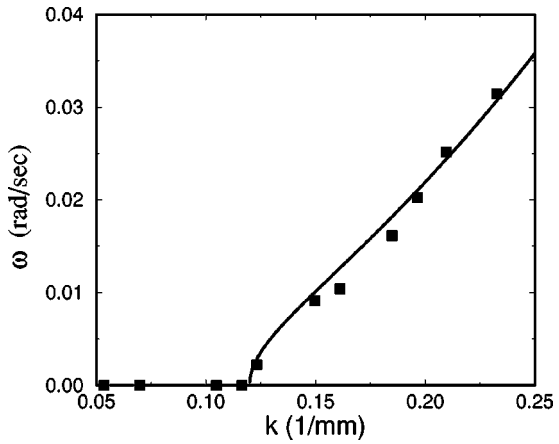

FIG. 3. Comparison of theoretical results ω vs k (solid line) with experimental data of Ref. [6] (squares). The values of parameters are the following: $\epsilon=0.0015$, $D=580\epsilon$ mm^2/sec, and $\delta=250\epsilon$ mm^2/sec, $\alpha=8\epsilon$ 1/sec.

ture of the flux Eq. (5) still may be correct, the values of $\tan\theta_{1,2}$ may be rather different from static value due to dilation effects. Thus, as a rough estimate we will take $\beta\sim O(1)$. Certainly, detailed experimental study is necessary to clarify this point.

Using expression (36), we can estimate α assuming that the dynamic angle of repose $\theta^*\approx 45°-60°$ for $C=0$ (compare [17]) and $\theta_0\approx 30°$. Thus, we get $\alpha=\epsilon\Omega(R^2-r_0^2)/2/(\tan\theta^*-\tan\theta_0)\approx(500-600)\epsilon$ mm^2/sec and $\overline{\alpha}=8\epsilon\,\mathrm{sec}^{-1}$. For $\kappa=0$ the diffusion coefficient D_θ assumes the value of $D_\theta\approx 200\epsilon$ mm^2/sec. Depending on the value of κ, D_θ can be much smaller. If the diffusion constants K_1 and K_2 for both components are different, which is typically the case for the grains of different size, we can assume that $\eta=(K_1-K_2)/(K_1+K_2)\sim O(1)$.

Using Eq. (35) we obtain the estimate for $\delta\approx(200-250)\epsilon$ mm^2/sec. Assuming that the diffusion coefficients D_c, D_θ are small compared to D, we can estimate the coefficient D independently from available experimental data. From Eq. (40) we obtain the imaginary part of λ, or the frequency of traveling waves, using that $D_\theta\sim D_c$:

$$\omega=\mathrm{Im}\,\lambda\approx\sqrt{D\overline{\delta}k^4-\overline{\alpha\beta\delta}k^2-\overline{\alpha}^2/4}. \tag{45}$$

This quantity was directly measured in the experiment [6]. In order to make an order of magnitude estimate, we take $D_c=D$. The numerical values of parameter D and relaxation parameter ϵ we extract from fitting the experimental dispersion relation $\omega(k)$. The onset of oscillatory behavior in the experiment occurred at the wave number $k^*=0.12$ mm^{-1}. Using Eq. (45) and estimated values for the parameters $\overline{\alpha},\delta$, we find $D\approx(550-650)\epsilon$ mm^2/sec.

Fitting of the slope of the experimental curve results in a very small value of parameter $\epsilon=0.0015$ (see Fig. 3). Presumably, this small value of ϵ is the indication of the fact that the segregation occurs in a very thin fluidized layer (one particle thick) at the free surface of rotating drum. Indeed, the parameter ϵ is of the order of the ratio of the particle radius to the radius of the drum.

VII. DYNAMICS OF SEGREGATION NUMERICAL RESULTS.

In order to simplify the numerical study of Eqs. (34) and reduce the number of parameters it is convenient to perform the scaling of the variables

$$\begin{aligned} t&\to\overline{\alpha}t,\\ z&\to z\sqrt{\overline{\alpha}/D_\theta},\\ \Theta&\to\delta/D_\theta\Theta,\\ f&=\beta\delta/D_\theta,\\ \gamma&=D\delta/D_\theta^2,\\ \nu&=D_c/D_\theta. \end{aligned} \tag{46}$$

This scaling casts Eqs. (34) in the dimensionless form

$$\partial_t\Theta=-\Theta+fC+\gamma\partial_z^2C+\partial_z^2\Theta, \tag{47}$$

$$\partial_tC=-\partial_z(1-C^2)\partial_z\Theta+\nu\partial_z(1-\eta C)\partial_zC. \tag{48}$$

Using the estimates for the parameters $\alpha, D_c, \delta, \beta$ from the previous section for the experiment of Ref. [6], we assume that D_θ is smaller or equal to D_c, D, δ. We obtain the following estimates for the values for the dimensionless parameters of Eqs. (48): $\gamma=2-20$ and $\nu\sim 1-3$. In order to have size segregation we have to choose $f>\nu$.

Numerical simulations of Eqs. (47) and (48) were performed using the pseudospectral split-step method. Periodic boundary conditions were implemented, except in the situation described in Fig. 7(b) where we used no-flux boundary conditions. We used 512 mesh points in our numerical procedure. At first we consider the case of $\eta=0$. Roughly speaking, the main effect of the nonlinearity related to ηC is the decreasing of ν. Simulations with $\eta\neq 0$ are presented later.

The dynamics of the initially preseparated states in a system with size $L=60$ is shown in Fig. 4. For initial perturbations with wave number $k>k_*$, in agreement with experiments [6], short-wave initial perturbations produce decaying standing waves, which later are replaced by long-wave quasistationary bands [Fig. 4(a)]. For initial perturbations with wave number smaller than k_* but larger than the optimal wave number k_m corresponding to the maximal growth rate Reλ, there are no transient oscillations. Rather there occurs some initial merging of bands leading to the optimal wave number selection [Fig. 4(b)]. After initial saturation, the bands are separated by sharp interfaces which are very weakly attracted to each other. In fact, in simulations with parameters corresponding to Fig. 4(a) we were not able to detect interface merging at all in a reasonable simulation time. However, at higher rates of diffusion and dissipation, corresponding to different experimental conditions (rotation frequency, filling factor, etc.), the interaction becomes more significant, and it leads to band merging and overall pattern coarsening [see Fig. 4(c)]. In Fig. 5, we present the number of bands as a function of time for this run.

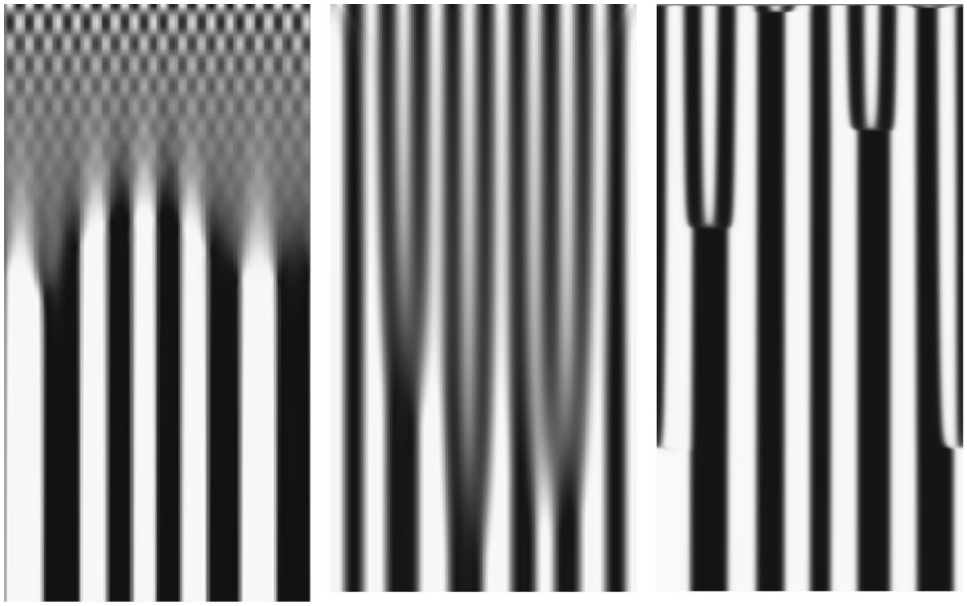

FIG. 4. Space-time diagrams of the evolution of the preseparated state $[C(z,0)=C_0+C_i\cos(k_0 z)]$ with $C_0=0$, $C_i=0.95$; spatial dimension $(0<z<30)$ plotted along the horizontal axis, time increases from top to bottom; (a) initial transient for $k_0=3.58>k_*$, $0<t<1.25$. At times $t<0.375$ the initial perturbations excite the decaying standing wave (superposition of left- and right-traveling waves), and at larger times $t>0.375$, aperiodic segregated bands emerge. Parameters of the model are: $\nu=0.5$, $\gamma=100$, $f=40$, and $L=30$; (b), same parameters, but for smaller wave number of initial perturbations, $k_0=1.6<k_c$; (c) space-time diagram for long-time evolution, band merging, and coarsening during long-time evolution $(0<t<5000)$ at higher diffusion constants, parameters $\nu=1.6, \gamma=4, \quad f=2, \quad L=140$.

We also solved Eqs. (47) and (48) for $\eta\neq 0$. The results are shown in Fig. 6. Although on a qualitative level the behavior is similar to that for $\eta=0$, some new features emerge. The transient oscillatory behavior arises at some threshold value of average concentration difference C_0. As we can see from Fig. 6, there are no oscillations for $C_0=-0.2$ and $C_0=0$, whereas for $C_0=0.5$ the oscillations are well-pronounced (all other parameters are kept the same). As we already mentioned in the Sec. VI, the explicit dependence of the diffusion coefficient of the concentration in Eq. (48) is one of the mechanisms for the threshold behavior of transient oscillations as the function of concentration difference C, observed in experiments in Ref. [6].

Zik *et al.* [4] have found experimentally that periodic modulation of the drum radius along its axis leads to locking the band structure to the drum periodicity: larger particles are concentrated in the necks, whereas smaller beads end up in the bellies. Equations (47) and (48) can be easily modified to study the effect of variable radius on the band formation. Generally, the z dependence of R affects all the parameters of the one-dimensional model (31), (32). However, assuming that radius modulation is small $R=R_0+R_1(z), R_1/R_0\ll 1$, one can linearize the equations with respect to R_1. In this case the main contribution comes from explicit dependence of the local terms $\sim\alpha/(R^2-r_0^2)(\tan\theta-\tanh\theta_0-\beta C)$ in Eq. (29). All terms involving the derivatives of θ, C and R_1 can be neglected as formally higher order ones. The expansion with respect to R_1 in Eq. (29) results in the additional term,

$$\frac{4\alpha R_0 R_1(z)}{(R_0^2-r_0^2)^2}(\tan\theta^*-\tan\theta_0-\beta C) = \frac{4\alpha R_0 R_1(z)}{(R_0^2-r_0^2)^2}\left(\frac{\epsilon\Omega(R_0^2-r_0^2)}{2\alpha}-\beta C\right). \tag{49}$$

Typically, the last term in Eq. (49) is smaller numerically than the first term because $\beta\sim 0.1\ldots 0.2$ whereas the first term is numerically $0.7\ldots 1$. Thus, we can neglect βC compared to the first term. After rescaling the variables according to Eq. (46) we obtain the equation

$$\partial_t\Theta=r_1(z)-\Theta+fC+\gamma\partial_z^2 C+\partial_z^2\Theta, \tag{50}$$

$$\partial_t C=-\partial_z(1-C^2)\partial_z\Theta+\nu\partial_z(1-\eta C)\partial_z C, \tag{51}$$

where

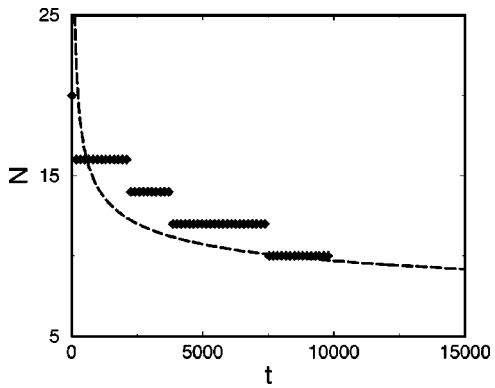

FIG. 5. Number of fronts N as a function of time (diamonds) and its fit by a function $N=70/(\ln t-2.5)$ (long-dashed line). Parameters correspond to Fig. 4(c).

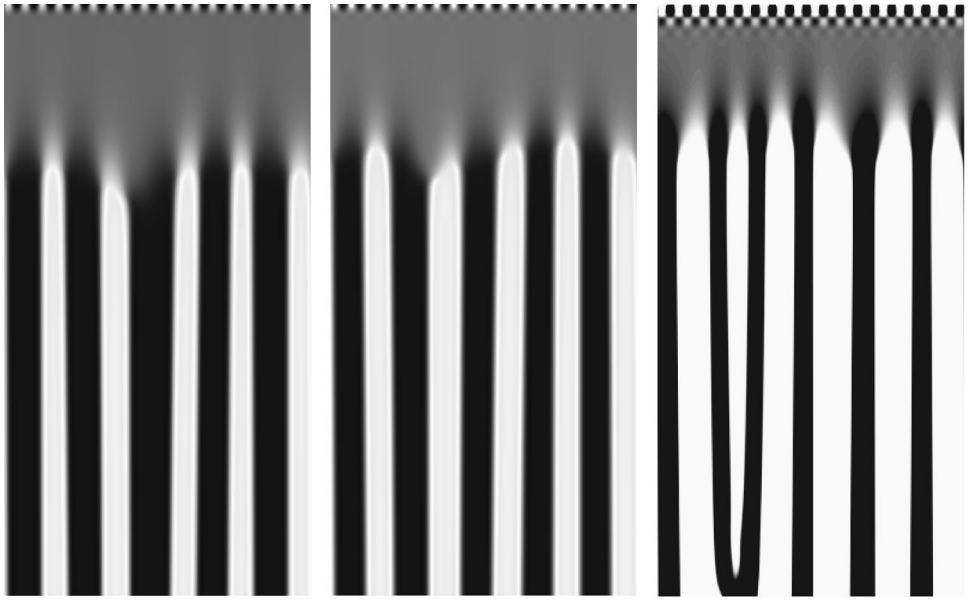

FIG. 6. Space-time diagrams of the evolution of the pre-separated state for different values of C_0 and $\eta=1$ for $\nu=3$, $f=40$, $L=40$, and $\gamma=10$. (a) $C_0=-0.2$, (b) $C_0=0$ and (c) $C_0=0.5$.

$$r_1=\frac{2\epsilon\Omega\,\delta R_0^2}{\overline{\alpha D}_\theta(R_0^2-r_0^2)}\,\frac{R_1(z)}{R_0}. \tag{52}$$

Figure 7(a) shows the results of the numerical solution of Eqs. (50) and (51) for sinusoidal modulation of the radius, $r_1=R_m\sin K_0 z$. We indeed observed locking of the band structure by the radius periodicity. Moreover, in agreement with experiment, minima of R (necks) correspond to the minima of C, or particles with smaller repose angle (presumably, large smooth particles). Using the same equations, one can also predict the effect of a monotonic change of the drum radius along the axis. If we take $R(z)=R_0+sz$, numerical simulations show that the bands quickly merge and complete separation occurs. Large particles are accumulated in the narrow end of the conic drum, and small particles are moved in the opposite end [see Fig. 7(b)]. Note that a similar effect can be anticipated for a slight tilted cylindrical tube. Indeed, the tilt leads to the axial dependence of the filling ratio $\Phi(z)$, or $r_0(z)$. Since r_0 enters the equations of motion together with R, decreasing r_0 (at the lower end of the tilted tube) is equivalent to increasing R, so small particles should accumulate at the lower end of the drum. Zik *et al.* [4] observed fast separation of the binary mixture in a drum with a helicoidal shape. Although the cross section of the drum remains almost circular with the fixed radius, the helicity leads to redistribution of granular material along the drum, and to variable $r_0(z)$, as in a conic or tilted drum. Therefore, we can speculate that the observed fast separation in a helicoidal is explained by our model as well.

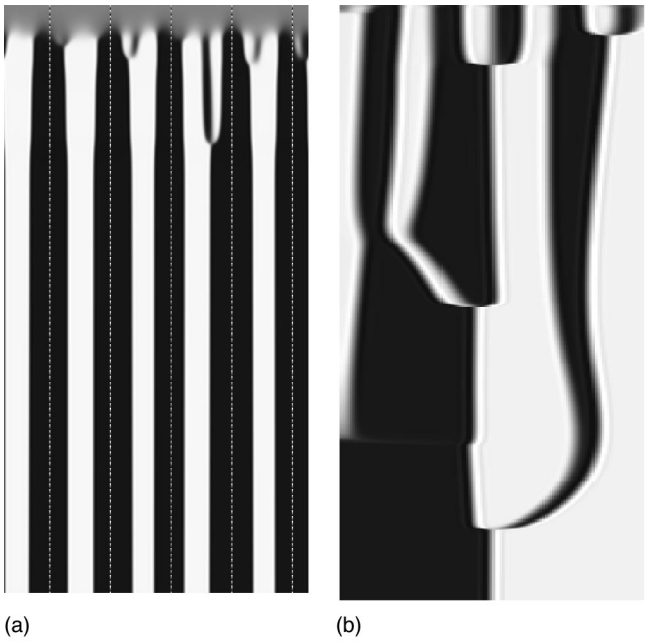

FIG. 7. (a) Band locking in the drum with modulated radius, Eqs. (50) and (51), for $\nu=2$, $\eta=0$, $\gamma=2$, $f=20$, $L=40$, $r_1=0.4\sin K_0 z$, $K_0=10\pi/L$, $0<t<50$. Dotted lines indicate the positions of minimal radius (necks). (b) Fast segregation occurred in the ''inclined'' drum, described by Eqs. (50) and (51) for $\nu=2$, $\eta=0$, $\gamma=2$, $f=20$, $L=50$, and $r_1=sz$, $s=4$, $0<t<20$, no-flux boundary conditions.

VIII. LONG-TIME EVOLUTION OF THE SEGREGATED STATE. FRONTS INTERACTION

Fronts separating bands of different grains can be found as stationary solutions of Eqs. (47) and (48). For simplicity we consider the case of $\eta=0$. In an infinite system one finds from stationary Eq.(48) $\Theta=\Theta_0+\nu G(c)$, where

$$G(c)=\int[1-C^2]^{-1}dC=-\frac{1}{2}\ln\frac{1-C}{1+C}$$

and Θ_0 is an integration constant. Plugging this expression into Eq. (28), we obtain the second order differential equation for C (for a symmetric solution one chooses $\Theta_0=0$),

$$\frac{d}{dz}\left[\left(\gamma+\frac{\nu}{1-C^2}\right)\frac{dC}{dz}\right]+fC+\frac{\nu}{2}\ln\frac{1-C}{1+C}=0. \tag{53}$$

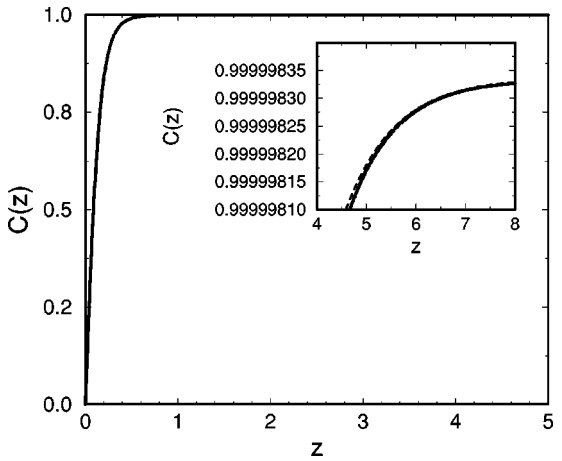

FIG. 8. Front solution to Eq. (53) for $\gamma=0$, $\nu=1$, and $f=7$. Inset: analytical expression Eq. (A21) (dashed line) and numerical solution (solid line).

It is easy to see that this equation possesses an interface solution. The asymptotic behavior of this solution can be found in the limit $\nu \ll f$, i.e., very small Fick diffusion in our notation, when the states on both sides of the interface are well segregated ($|C(z\to\pm\infty)|\to\pm 1$). In this limit, far away from the interface, we obtain

$$1-|C|\to\xi\exp(-|z|/d_0), \tag{54}$$

where

$$d_0=\left(1+\frac{4\gamma}{\nu}\exp-\frac{2f}{\nu}\right)^{1/2}\approx 1$$

with the prefactor $\xi=4f/\nu\exp[-2f/\nu]$ which is *exceedingly small* for $f_0\gg\nu$ (see the Appendix). The front solution to Eq. (53) is shown in Fig. 8. As one can see, there is excellent agreement between the numerical solution and the analytical asymptotic expression.

As follows from Eq. (54), already weak exponential interaction between the fronts is additionally attenuated by the very small factor ξ. This result could be anticipated, as in the absence of diffusion the nonlinearity $1-C^2$ drives the system towards complete segregation. This exponentially weak interaction between the neighboring fronts leads to exponentially long times for the front annihilation, $T\propto\exp(d/d_0)$, where d is the initial distance between fronts. For the multiband structure, the number of fronts N (proportional to the inverse average distance between fronts) decreases approximately as a logarithmic function of time [$N=1/d\sim 1/(\text{const}+d_0\ln T)$]. This dependence indeed agrees with our numerical simulations (see Fig. 5).

The time T for complete segregation (all bands merge) in the drum with the length L will be therefore exponentially large $T\sim\exp L$. Note that in the ''helicoidal'' drum [see the previous section, Eqs. (50) and (51)] the time for complete segregation is much smaller, $T\sim L/\nu$ only.

There is an interesting analogy between band merging in axial separation and phase ordering in one dimension. This process is often described phenomenologically by the Cahn-Hilliard equation [18]. As in the Cahn-Hilliard model, the order parameter of our system (concentration C) is a conserved quantity; therefore front interaction must conform to a global constraint. Moreover, our model reduces to the Cahn-Hilliard model in the limit of weak segregation $f\to\nu$. For a very long-time evolution we can assume that the concentration C enslaves the repose angle Θ. Thus we can drop the time derivative in Eq. (47) and express Θ explicitly in terms of C and its gradients. From Eq. (47) we obtain

$$\Theta\approx fC-(\gamma\partial_z^2C+\partial_z^2\Theta)\approx fC-(\gamma+f)\partial_z^2C. \tag{55}$$

Substituting Eq. (55) into Eq. (48) we obtain the generalized Cahn-Hilliard model

$$\partial_tC=-\partial_{zz}[(f-\nu)C-fC^3/3]-(\gamma+f)\partial_z[(1-C^2)\partial_{zzz}C], \tag{56}$$

which differs from the standard Cahn-Hilliard model only by the nonlinearity in the last term. In the limit $f\to\nu$ the asymptotic value of the front tends to 0. Therefore in this limit we can omit nonlinearity in the last term of Eq. (56), and obtain the standard Cahn-Hilliard model. In Ref. [15] the Cahn-Hilliard type equation with noise was applied to describe axial segregation. It was confirmed numerically, in agreement with experiment in Ref. [10], that an early stage of the band coarsening obeys a logarithmic law similar to our Eqs. (47) and (48).

Front solutions within the Cahn-Hilliard equation are found analytically as $C(Z)=C_0+\sqrt{3(f-\nu)/f}\tanh[d_0(z-z_0)]$. The problem of front interaction in a specific system with mass conservation within Cahn-Hilliard model has been recently considered in Ref. [19]. This analysis predicts that a single band of positive C in the sea of negative C (two fronts) can either annihilate or reach a stationary width depending on the initial distance between fronts. If a number of fronts is greater than 2, front interaction leads to their annihilation and pattern coarsening similar to the band merging in axial segregation.

IX. CONCLUSION

In conclusion, we developed a continuum description for the axial segregation of binary granular mixtures in long rotating drums. The model is obtained by averaging the mass transport equations for the two components under the assumption that the separation occurs only in the thin near-surface flow where the granular material is dilated, and simply advected by the bulk flow. The systematic averaging of transport equations results in a one-dimensional system which operates with only two local dynamical variables, relative concentration of two components, and dynamic repose angle. The dynamics of the reduced system shows a qualitative similarity with the experimental observations of initial transients and long-term segregation dynamics [4,3,6]. It captures both initial transient traveling waves and the subsequent onset of the band structure, followed by the slow coarsening process. Our theory agrees with the experimental observation of Ref. [6] that the threshold of the transient oscillatory behavior depends on the average concentration difference. In the framework of our system it is explained by the dependence of the concentration diffusion coefficient on C in Eq. (48).

The dispersion relation for the small-amplitude spatially

periodic perturbations with respect to the uniform state quantitatively agrees with the experimental measurements of Ref. [6] and was used for the fitting of unknown parameters of the one-dimensional system, Eqs. (34). In particular, the comparison of the theory with the experimental data implies that for a fast rotation speed the motion of the material in the bulk of the drum is quite different from the rigid-body rotation typically assumed for slowly rotating drums. Moreover, our model suggests that most of the particles are advected within the bulk, and only a very small fraction of particles, determined by our dimensionless parameter ϵ, is involved in the segregating motion within the thin near-surface layer.

Our model exhibits very slow coarsening of quasistatic band structure. Numerical simulations indicate that the time dependence of the number of bands is consistent with a logarithmic law. Such slow coarsening is typical for systems with exponentially weak attractive interaction among defects or interfaces, as in the phase ordering kinetics described by the one-dimensional Cahn-Hilliard model. This logarithmic coarsening of the quasistatic band structure deserves experimental verification.

Our simulations also showed that the model qualitatively reproduces more complicated phenomenology of the separation process reported in Ref. [4]. In particular, spatially periodic modulation of the drum radius R, leads to band locking at the loci of minima R (necks). Breaking of the $z \rightarrow -z$ symmetry by the term $\sim sz$, introduced in the rhs of Eq. (48), results in complete segregation, similarly to the dynamics of grains in the drum with helicoidal shape.

In the derivation of this model we explicitly assumed the absence of the radial segregation. This assumption is reasonable for narrow rapidly rotating drums where strong Fick diffusion prevents radial segregation. Obviously, a more elaborate three-dimensional model is needed to describe both radial and axial segregation within a unified framework for a drum with arbitrary radius and rotation speed.

ACKNOWLEDGMENTS

We thank S. Morris, J. Kakalios, and J. Goddard for useful discussions. This research was supported by the U.S. Department of Energy under Grant Nos. W-31-109-ENG-38, DE-FG03-95ER14516, DE-FG03-96ER14592, and by the NSF, STCS No. DMR91-20000.

APPENDIX: ASYMPTOTIC BEHAVIOR OF FRONT

We want to find asymptotic behavior for the front solution to Eq. (53). For simplicity we consider $\gamma=0$. To find an analytic solution we consider the case $f \gg \nu$. In this limit the fronts are very sharp, and we can apply the matching asymptotic expansion technique. We break the interval of integration in two pieces. In the first (inner) region we drop fC and solve the equation exactly, while in the outer region we keep fC but consider $C \rightarrow 1$.

Let us define a new variable

$$\zeta = \ln \frac{1-C}{C+1}, \tag{A1}$$

which yields

$$C = \frac{1-\exp\zeta}{1+\exp\zeta} = -\tanh \zeta/2. \tag{A2}$$

In the new variables Eq. (53) assumes the form

$$\frac{d^2\zeta}{dz^2} + \frac{2f}{\nu}\tanh\zeta/2 - \zeta = 0. \tag{A3}$$

After multiplying Eq. (A3) by $\partial_z \zeta$ and integrating we arrive at

$$(\zeta')^2 + \frac{8f}{\nu}\ln\cosh\zeta/2 - \zeta^2 = \text{const} = I_0. \tag{A4}$$

Constant I_0 we obtain from the boundary conditions that $\zeta \rightarrow \zeta_0$ for $z \rightarrow \infty$:

$$I_0 = \frac{8f}{\nu}\ln\cosh\zeta_0/2 - \zeta_0^2, \tag{A5}$$

where ζ_0 can be found from the equation

$$\frac{2f}{\nu}\tanh\zeta_0/2 = \zeta_0. \tag{A6}$$

From Eq. (A6) we obtain that $\zeta_0 \approx -2f/\nu$ if $C \rightarrow 1$ (alternatively, $\zeta_0 \approx 2f/\nu$ for $C \rightarrow -1$). Correspondingly, for I_0 we obtain

$$I_0 \approx \frac{4f^2}{\nu^2} - \frac{8f}{\nu}\ln 2 = \zeta_0^2 - 4|\zeta_0|\ln 2. \tag{A7}$$

The solution $\zeta(z)$ is implicitly given by the integral

$$\int \frac{d\zeta}{\sqrt{I_0 - \frac{8f}{\nu}\ln\cosh\zeta/2 + \zeta^2}} = z. \tag{A8}$$

After simple transformations integral Eq. (A8) assumes the form

$$I = \int_0^y \frac{dy}{\sqrt{1+y^2 - \frac{4}{|\zeta_0|}\ln[2\cosh(\zeta_0 y/2)]}} = z, \tag{A9}$$

where $y = \zeta/\zeta_0$.

We evaluate this integral using matching asymptotic technique. We present

$$I = I_1 + I_2, \tag{A10}$$

where $I_1 = \int_0^{y^*}$, $I_2 = \int_{y^*}^{y}$. In both intervals, $0 < y < y^*$ and $y^* < y \rightarrow 1$ we expand $\zeta_0^{-1} \log 2\cosh(\zeta_0 y/2)$ using different asymptotic representations.

First we will deal with I_2. For this integral we will use outer expansion, assuming that $|\zeta_0| y \gg 1$. It leads to the expression

$$I_2=\int_{y^*}^{y}\frac{dy}{\sqrt{1+y^2-2y-\frac{4}{|\zeta_0|}\exp(-|\zeta_0|y)}}. \quad \text{(A11)}$$

The last term in the integral $1/\zeta_0 \ln[1+\exp(-|\zeta_0|y)]$ can be neglected with respect to other terms y if

$$\frac{1}{|\zeta_0|}\ll y<1. \quad \text{(A12)}$$

In this interval, the integral I_2 is reduced to

$$I_2=-\ln(1-y)+\ln(1-y^*)=-y^*-\ln(1-y) \quad \text{for } y^*\ll 1. \quad \text{(A13)}$$

For the integral I_1 we expand $4/\zeta_0 \ln 2\cosh \zeta_0 y/2$ in the interval $|\zeta_0|y\ll 1$:

$$4/|\zeta_0|\ln 2\cosh \zeta_0 y/2\approx \frac{4\ln 2}{|\zeta_0|}+\frac{1}{2}|\zeta_0|y^2-\frac{1}{48}|\zeta_0|^3y^4+\frac{1}{720}|\zeta_0|^5y^6+\cdots. \quad \text{(A14)}$$

Keeping only the first two terms in the expansion, we obtain the integral

$$I_1=\int_0^{y}\frac{dy}{\sqrt{1-4/|\zeta_0|\ln 2-(|\zeta_0|/2-1)y^2+\cdots}}. \quad \text{(A15)}$$

This expansion is valid only if $0<y\ll|\zeta_0|^{-1/2}$, which overlaps with the interval (A12) on its outer limit. From Eq. (A15) we obtain

$$I_1\approx\left(\frac{2}{|\zeta_0|}\right)^{1/2}\arcsin(\sqrt{|\zeta_0|/2}y^*)=y^* \quad \text{for} \quad \sqrt{|\zeta_0|}y\ll 1. \quad \text{(A16)}$$

Combining I_1 and I_2 we see that y^* drops completely. We obtain

$$I=I_1+I_2=-\ln(1-y)=z. \quad \text{(A17)}$$

Finally, we obtain

$$1-\zeta/\zeta_0=\exp(-z). \quad \text{(A18)}$$

Now,we express ζ in terms of C using Eq. (A1) for $C\to 1$. Eq. (A1) for $C\to 1$ yields $\zeta_0=\ln(1-C_0/2)$. Representing $C=C_0-\xi$ one derives $1-C_0=2\exp[-2f/\nu]$. We have from Eq. (A1)

$$\zeta\approx\zeta_0+\xi/(1-C_0). \quad \text{(A19)}$$

It yields

$$\xi=\zeta_0(1-C_0)\exp(-z)=\frac{4f}{\nu}\exp\left[-\frac{2f}{\nu}\right]\exp(-z). \quad \text{(A20)}$$

Using Eq. (A20) we obtain an explicit asymptotic expression for C:

$$C=1-2\exp\left[-\frac{2f}{\nu}\right]-\frac{4f}{\nu}\exp\left[-\frac{2f}{\nu}\right]\exp(-z). \quad \text{(A21)}$$

If $f\gg\nu$, the prefactor of the asymptotics is exponentially small as

$$\exp\left[-\frac{2f}{\nu}\right].$$

[1] H. M. Jaeger, S.R. Nagel, and R. P. Behringer, Phys. Today **49**, 32 (1996); Rev. Mod. Phys. **68**, 1259 (1996).

[2] P. Umbanhowar, F. Melo, and H.L. Swinney, Nature (London) **382**, 793 (1996).

[3] K. M. Hill, A. Caprihan, and J. Kakalios, Phys. Rev. Lett. **78**, 50 (1997).

[4] O. Zik, D. Levine, S.G. Lipson, S. Shtrikman, and J. Stavans, Phys. Rev. Lett. **73**, 644 (1994).

[5] F. Cantelaube and D. Bideau, Europhys. Lett. **30**, 133 (1995); E. Clément, J. Rajchenbach, and J. Duran, *ibid.* **30**, 7 (1995); K.M. Hill and J. Kakalios, Phys. Rev. E **49**, 3610 (1994); **52**, 4393 (1995).

[6] K. Choo, T.C.A. Molteno, and S. W. Morris, Phys. Rev. Lett. **79**, 2975 (1997); K. Choo, M.W. Baker, T.C.A. Molteno, and S.W. Morris, Phys. Rev. E **58**, 6115 (1998).

[7] J. B. Knight, H. M. Jaeger, and S. Nagel, Phys. Rev. Lett. **70**, 3728 (1993).

[8] H. A. Makse, P. Cizeau, and H. E. Stanley, Phys. Rev. Lett. **78**, 3298 (1997); T. Boutreux and P.-G. de Gennes, J. Phys. I (France) **6**, 1295 (1996).

[9] J. P. Koeppe, M. Enz, and J. Kakalios, Phys. Rev. E **58**, R4104 (1998).

[10] V. Frette and J. Stavans, Phys. Rev. E **56**, 6981 (1997).

[11] R. Chicharro, R. Peralta-Fabi, and R. M. Velasco, in *Powders and Grains '97*, edited by R. P. Behringer and J. T. Jenkins (A. A. Balkema, Rotterdam, 1997), p. 479.

[12] I. Aranson and L. Tsimring, Phys. Rev. Lett. **82**, 4643 (1999).

[13] L. Prigozhin and H. Kalman, Phys. Rev. E **57**, 2073 (1998).

[14] T. Elperin and A. Vikhansky, Europhys. Lett. **43**, 17 (1998); **42**, 619 (1998).

[15] B. Levitan, Phys. Rev. E **58**, 2061 (1998).
[16] P.-Y. Lai, L.-C. Jia, and C.K. Chan, Phys. Rev. Lett. **79**, 4994 (1997).
[17] K.M. Hill, J. Kakalios, K. Yamane, Y. Tsuji, and A. Caprihan, in *Powders and Grains '97* (Ref. [11]).
[18] J. W. Cahn and J. E. Hilliard, J. Chem. Phys. **28**, 258 (1958).
[19] A. A. Fraerman, A. S. Melnikov, I. M. Nefedov, I. A. Shereshevskii, and A. V. Shpiro, Phys. Rev. B **55**, 6316 (1997).